Progress In Electromagnetics Research Letters, Vol. 40, 81–92, 2013

NOVEL TRI-BAND BANDPASS FILTER USING STUB-LOADED SHORT-ENDED RESONATOR

Xiu Yin Zhang*, Li Gao, Ze Yu Cai, and Xiao-Lan Zhao

School of Electronic and Information Engineering, South China University of Technology, Guangzhou 510640, China

Abstract—This paper presents a tri-band bandpass filter (BPF) using a novel stub-loaded resonator. Different from other stub-loaded resonator, this resonator utilized a short-ended main transmission line and a centerly-loaded open stub. The resonator is theoretically analyzed. The first three resonant frequencies can be individually adjusted and this enables the convenient designs of tri-band BPFs. For demonstration, a tri-band BPF is implemented. Transmission zeros are created close to each passband edge, resulting in high skirt selectivity. Comparisons of the measured and simulated results are presented to verify the theoretical predications.

1. INTRODUCTION

As important building blocks of wireless communication systems, bandpass filters (BPFs) have gained a lot of attention. Much research has been conducted, such as UWB filters [1–4], miniaturized filters [5, 6] and multi-band filters [7–24]. With the deployment of multi-band wireless system, the capabilities of accessing multi-band frequencies are needed to reduce the number of components in RF systems. For tri-band BPF designs, a typical method is to use tri-section stepped-impedance resonators (SIRs) [11, 12]. By controlling the electronic length ratios and impedance ratio, tri-band responses can be obtained. However, the resonant frequencies are dependent and the degrees of freedom are limited. Another typical way to design tri-band BPFs is to combine several sets of resonators [13–17]. In [13], three sets of resonators are utilized and each set of resonator forms a passband. Thus, a tri-band response can be achieved. In [14], one resonator is used to realize one passband and the other set of resonator is employed

Received 2 April 2013, Accepted 16 April 2013, Scheduled 13 May 2013

* Corresponding author: Xiu Yin Zhang (zhangxiuyin@hotmail.com).

to obtain two passband. Using this method, the passband frequencies and bandwidths can be easily controlled. However, it is difficult to reduce the filter size. Recently, stub-loaded resonators are combined with other resonators to obtain tri-band responses [18, 19].

In multi-band filter designs, resonators are crucial building elements. In the reported works, open-ended microstrip resonators are dominant. In fact, the short-ended resonators process certain advantages and can exhibit some characteristics different from the open-ended counterparts. Therefore, this topic is starting to get attention. In [8], stub-loaded short-ended resonators are adopted to design dual-band BPFs with different frequency ratios. Besides dual-band filters, it also can be used to design tri-band filters.

In this paper, a novel short-ended resonator is proposed to design a compact tri-band BPF with high selectivity. The first three resonant frequencies can be individually adjusted. Using the proposed resonators together with source-load inter-digital coupling structures, a compact tri-band BPF with high selectivity is designed. The design methodology and experimental results are presented.

2. ANALYSIS OF THE PROPOSED TRI-BAND FILTER

2.1. Resonator Analysis

Figure 1 illustrates the configuration of the tri-band BPF. The filter is folded to reduce the circuit size. They are connected together using a via hole as the coupling structure. Inter-digital coupling is realized between the input and output, forming source-load coupling. Several coupling fingers are utilized to provide sufficient degrees of freedom to control the locations of the transmission zeros generated by the source-load coupling.

This microstrip filter consists of two short-ended resonators, as shown in Fig. 2(a). The horizontal part is the short-ended transmission line with characteristic admittance of Y_{10}. The stepped-impedance stub is loaded at the line center, with the length and characteristic admittance of L_{12}, Y_{12} and L_{13}, Y_{13}, respectively. The structure is symmetrical and thus odd-even-mode analysis can be utilized to characterize it.

For odd-mode excitation applied to Feed 1 and 2 as shown in Fig. 2(a), there is a voltage null at the center plane of the resonator. Thus we can get the equivalent circuit as shown in Fig. 2(b). The resulting input admittance for odd-mode is given by

$$Y_{in,odd} = -j\frac{Y_{10}}{\tan\theta_{10}} - j\frac{Y_{10}}{\tan\theta_{11}} \tag{1}$$

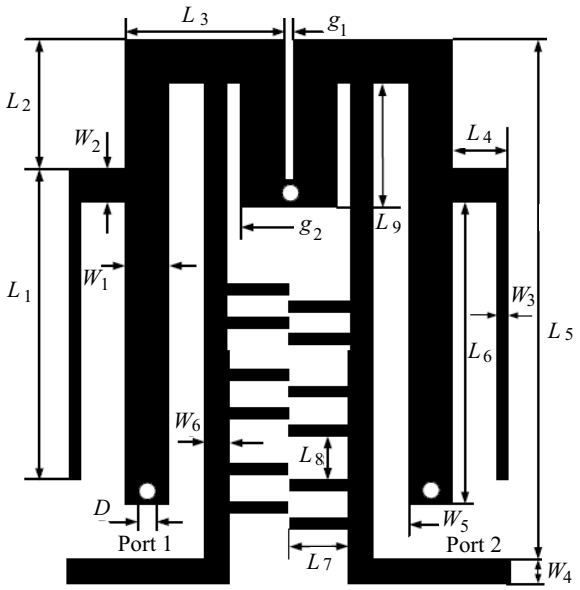

Figure 1. Configuration of the tri-band BPF.

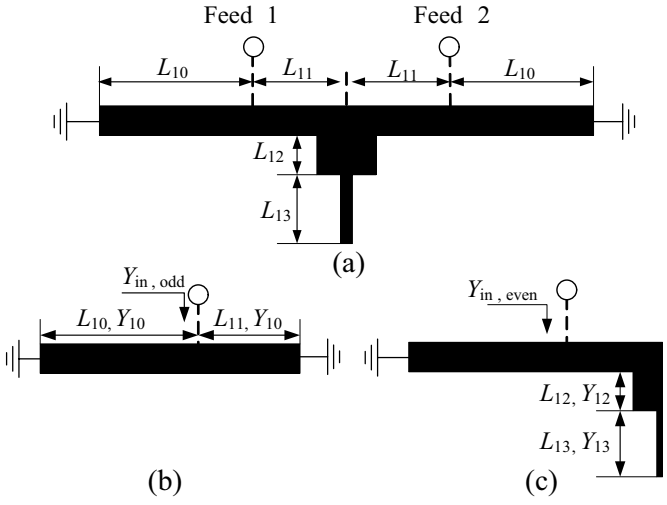

Figure 2. (a) Configuration of the proposed resonator. (b) Odd-mode equivalent circuit. (c) Even-mode equivalent circuit.

where $\theta_{10} = \beta L_{10}$, $\theta_{11} = \beta L_{11}$. From the resonant condition that the imaginary part $Y_{in,odd}$ is equal to zero, the odd-mode resonant frequencies can be deduced as:

$$f_{odd} = \frac{nc}{L\sqrt{\varepsilon_{eff}}} \tag{2}$$

where $L = 2(L_{10} + L_{11})$, $n = 1, 2, 3, \ldots$, c is the velocity of light in space, and ε_{eff} is the effective permittivity. It is seen that the odd-mode resonant frequencies are not affected by the stub dimensions. In this design, the fundamental f_{odd} is used as the third passband frequency and the overall electric length of L_{10} and L_{11} is half wavelength at this frequency.

If even-mode excitation is applied, the equivalent circuit can be obtained as shown in Fig. 2(c). Ignoring the discontinuity of the junction, the input admittance can be approximately expressed as

$$Y_{in,even} = -j\frac{Y_{10}}{\tan\theta_{10}} + Y_{10}\frac{\frac{jY_{12}(Y_{12}\tan\theta_{12}+Y_{13}\tan\theta_{13})}{Y_{12}-Y_{13}\tan\theta_{12}\tan\theta_{13}} + j2Y_{10}\tan\theta_{11}}{2Y_{10} - Y_{12}\tan\theta_{11}\frac{Y_{12}\tan\theta_{12}+Y_{13}\tan\theta_{13}}{Y_{12}-Y_{13}\tan\theta_{12}\tan\theta_{13}}} \tag{3}$$

where $\theta_{12} = \beta L_{12}$, $\theta_{13} = \beta L_{13}$. The resonance condition is $Y_{in,even} = 0$. For simplicity, some special cases are assumed. In the case of $Y_{12} = 2Y_{10}$, it becomes

$$\frac{2Y_{10}}{Y_{13}} = \tan\theta_{13}\tan(\theta_{10} + \theta_{11} + \theta_{12}) \tag{4}$$

Assuming that $R_Z = 2Z_{13}/Z_{10} = 2Y_{10}/Y_{13}$, then we can get

$$\tan\theta_{13}\tan\theta = RZ \tag{5}$$

where $\theta = \theta_{10} + \theta_{11} + \theta_{12}$. If $\theta = \theta_{13}$, the ratio of the second resonant frequency to the first one can be written as

$$\frac{f_2}{f_1} = \frac{\pi}{\tan^{-1}\sqrt{RZ}} - 1 \tag{6}$$

From the analysis, it is seen that there are two resonant frequencies f_1 and f_2, which are used as the first and second passband frequencies in this filter design.

In case of $\theta \neq \theta_{13}$, $Y_{12} \neq 2Y_{10}$, the analytical solutions are not available. Hence, simulation is carried out to illustrate it. Fig. 3 shows the passband frequencies against the stub dimensions. As can be seen in Fig. 3(a), when the stub length increases, the first and second passband frequencies decrease and the third one is maintained constant, which fits Equation (1). As indicated in Fig. 3(b), the first passband frequency decreases when the width W_3 becomes wider, while the second passband frequency changes very slightly. It indicates that the resonant frequencies can be individually controlled.

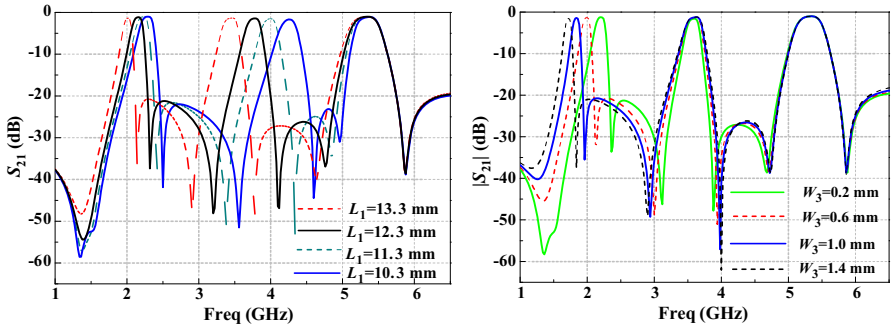

Figure 3. (a) Passband frequencies against the stub length L_1 ($W_3 = 0.4$ mm). (b) Passband frequencies against the stub width W_3 ($L_1 = 12.3$ mm).

2.2. Filter Design

For BPF design, frequencies and bandwidths are two important parameters. Using the proposed resonators, the frequencies can be individually controlled, as stated in the previous section. For bandwidth, it is mainly determined by coupling coefficient k and external quality factor Q_e. The k is determined by the coupling between the two resonators. Therefore, The coupling region with the gap g_1 and length L_9 as well as the via determine the k. Based on the simulation results, the k can be extracted by [24]:

$$k = \frac{f_2^2 - f_1^2}{f_2^2 + f_1^2} \tag{7}$$

where f_2 and f_1 are two split resonant frequencies near the resonant frequency.

Figures 4(a)–(c) depicts the k_i at the passband frequency f_i with various g_1, L_9 and d, respectively. Where $i = 1, 2, 3$ corresponds to the first, second and third passband. It can be observed that k at the three passbands becomes small with large g_1 and d. Large L_9 results in large k_1, k_2 and small k_3. Different combinations of g_1, L_9 and d result in various k at the three passbands, which can fulfill different requirements.

As for Q_e, it is mainly determined by the tap position of the ports, the coupling gap g_2 and the width of feeding lines W_6. The Q_e also can be extracted by simulation [24]

$$Q_e = \frac{f_0}{\Delta f_{\pm 90^\circ}} \tag{8}$$

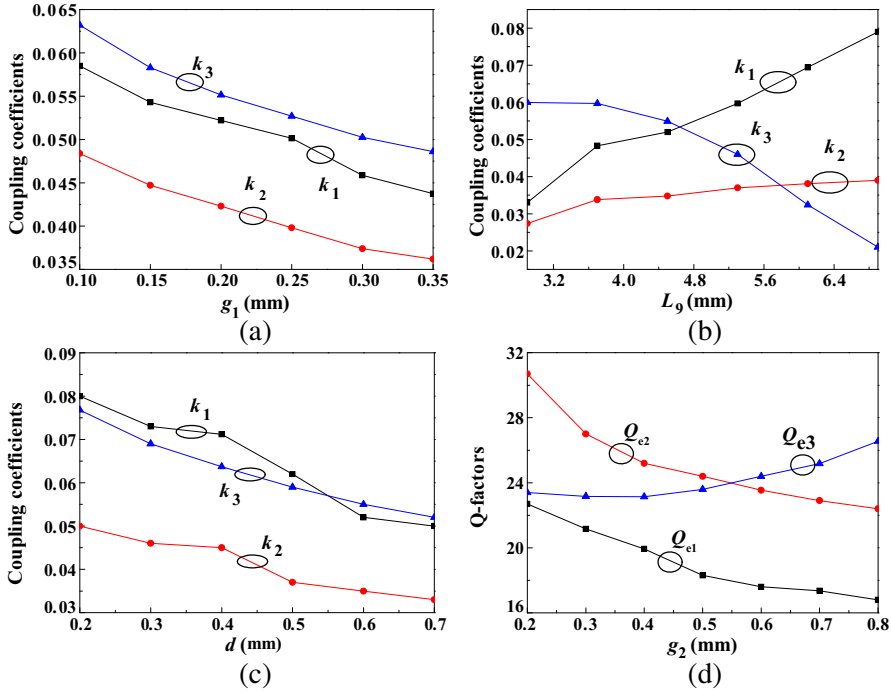

Figure 4. (a) k against gap g_1, (b) k against length L_9, (c) k against via diameter d and (d) Q_e against gap g_2.

where $\Delta f_{\pm 90^\circ}$ denotes the bandwidth of which the phase shifts $\pm 90^\circ$ with respect to the phase of resonant frequency. Fig. 4(d) describes the relation between Q_e and g_2, where Q_{ei} is the Q_e at the passband frequency f_i. Meanwhile, the length L_2 can be used for fine tuning Q_e at the first two passbands because it will affect the Q_e at the first two passbands and has no impact on the Q_e at the third passband. Fig. 5 shows the simulated results with various L_2. It can be observed that a larger L_2 results in smaller bandwidth of the first passband and larger bandwidth of the second passband, while the third passband keeps unchanged. Thus, flexible combination of the tap position, coupling gap, feeding line width as well as L_2 can results in various Q_e at the three passbands.

The inter-digital coupling fingers are used to form source-load coupling. The coupling schematic is shown in Fig. 6. There are two coupling paths. The coupling between the source and load is electric coupling whereas the coupling between the two resonators is magnetic coupling. As addressed in [25], if the signals from the two paths

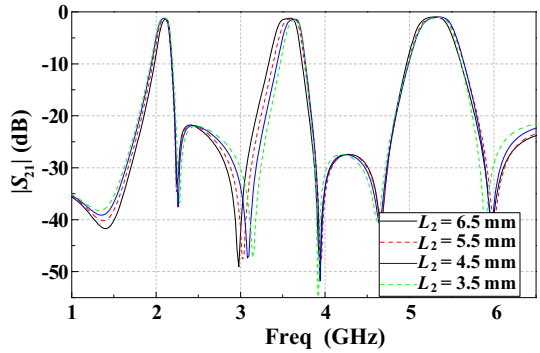

Figure 5. $|S_{21}|$ against the length L_2.

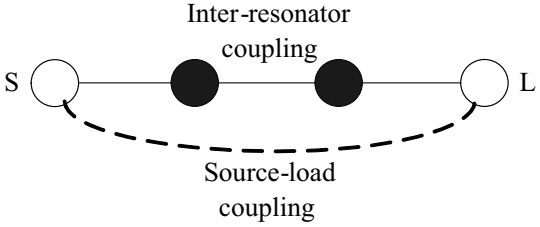

Figure 6. Coupling schematic.

are out of phase and equal in magnitude at certain frequencies, then they can be cancelled out and thus transmission zeros are generated at these frequencies. Therefore, due to the source-load coupling, the transmission zeros can be generated. Also, the inter-digital coupling can be used to control the location of the transmission zeros. This is illustrated in Fig. 7. With various inter-digital coupling dimensions, the location of the transmission zeros is different. This is because the source-load coupling strength and phase shift are different with various inter-digital coupling dimensions, while the signals from the main coupling are fixed. If the coupling is too weak, there is no transmission zero.

Based on the analysis, the design methodology is as follows. The first step is to determine the resonator length. The whole length of the short-ended transmission line is one wavelength at the third (upper) passband f_3. After that, we can adjust the length of the stepped-impedance stub to achieve the required first two passband frequencies. The overall electric length of $L_1 + L_4 + L_6$ corresponds to a quarter-wavelength stepped-impedance resonator with the resonant frequencies

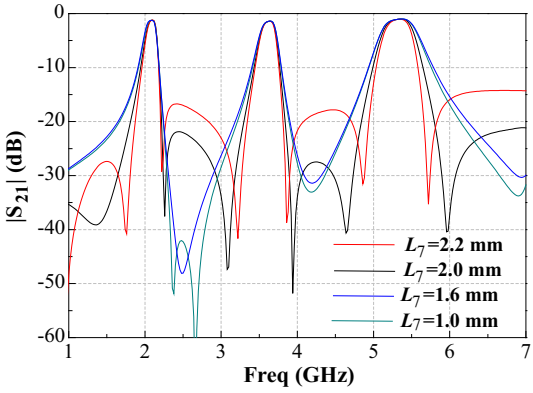

Figure 7. Simulated $|S_{21}|$ against L_7.

of f_1 and f_2. The frequency ratio is determined by the line width ratio and the width W_3 can be altered to attain the desired first passband frequency f_1. The second step is to select various combination of the gap size g_1, L_9 and the via diameter to obtain the required k at the three passbands. Similarly, the tap position, coupling gap size between the feeding line and the resonator, the feeding line width are used to fulfill the requirement of the Q_e. The third step is to determine the number and length of the inter-digital coupling figures to generate transmission zeros. Finally, fine tuning is performed to obtain overall good performance.

3. FILTER IMPLEMENT

For demonstration, a tri-band BPF is implemented. The fractional bandwidths are determined as 10%, 6.5% and 9%. The Q_e and k are as follows. $Q_{e1} = 14$, $k_1 = 0.1$, $Q_{e2} = 21.6$, $k_2 = 0.065$, $Q_{e3} = 15.6$, $k_3 = 0.09$. In this design, the substrate has a relative dielectric constant of 6.15 and a thickness of 0.635 mm. The dimensions are optimized as follows: $L_1 = 12.3\,\text{mm}$, $L_2 = 4.6\,\text{mm}$, $L_3 = 5.8\,\text{mm}$, $L_4 = 2\,\text{mm}$, $L_5 = 19.8\,\text{mm}$, $L_6 = 12\,\text{mm}$, $L_7 = 2\,\text{mm}$, $L_8 = 1.6\,\text{mm}$, $L_9 = 4.4\,\text{mm}$, $W_1 = 1.6\,\text{mm}$, $W_2 = 1.2\,\text{mm}$, $W_3 = 0.4\,\text{mm}$, $W_4 = W_6 = 0.92\,\text{mm}$, $W_5 = 1.5\,\text{mm}$, $g_1 = 0.2\,\text{mm}$, $g_2 = 0.3\,\text{mm}$, $D = 0.6\,\text{mm}$. The overall size is $0.29\lambda_g \times 0.25\lambda_g$, where λ_g is the guide-wavelength of the first passband frequency. The photograph of the fabricated filter is shown in Fig. 8.

The simulation and measurement are accomplished by using IE3D and 8753ES network analyzer, respectively. Fig. 9 shows the simulated

Figure 8. Photograph of the fabricated filter.

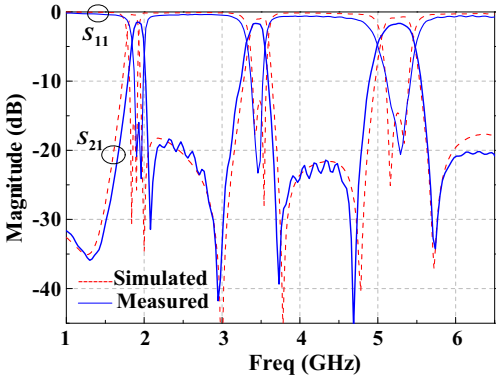

Figure 9. Simulated and measured results of the tri-band BPF.

and measured results. A slight difference is observed, which may be due to the fabrication error. The first passband frequency is located at 1.95 GHz with 3 dB bandwidth of 190 MHz or 9.7%. The measured minimum insertion loss is 1.5 dB, and the return loss is better than 15 dB. The second passband frequency is centered at 3.46 GHz. The 3 dB bandwidth is 220 MHz or 6.4%, which covers the WiMAX system. The measured minimum insertion loss is 1.2 dB, and the return loss is better than 20 dB. The third passband center frequency is 5.25 GHz with fabricated 3 dB bandwidth of 470 MHz or 9%, which covers the WLAN system. The measured minimum insertion loss is 1.6 dB, and the return loss is 21 dB.

Six transmission zeros are generated close to the passband edges due to the source-load coupling, which greatly improve the skirt selectivity. For demonstration, the responses of the filter with and without the interdigital coupling are illustrated in Fig. 10. It can be observed that if interdigital coupling is removed, there is no transmission zero. It is indicated that these six transmission zeros are created due to the source-load coupling.

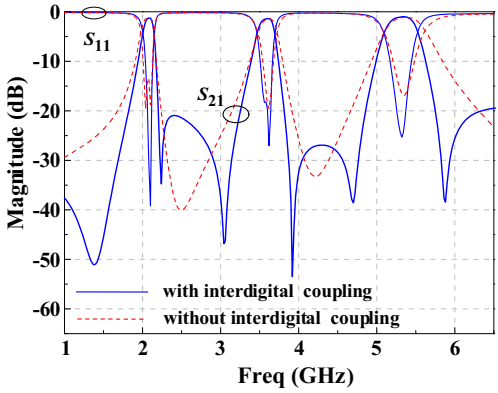

Figure 10. Filter responses with and without interdigital coupling.

4. CONCLUSION

This paper presents a high-selectivity tri-band BPF using one set of stub-loaded short-ended resonators. Both theory and experiments are provided. Triple resonance modes with individually controlled frequencies have been observed, and thus the resonators are attractive for tri-band BPF designs. A demonstration filter with compact size has been implemented. For each passband, two transmission zeros are created close to each passband edge, ensuring high selectivity.

ACKNOWLEDGMENT

This work was supported by the Natural Natural Science Foundation of China and Guangdong under Grant. 61271060, U103500 and S2012010008742 and by NECT-10-0402.

REFERENCES

1. Sarkar, P., M. Pal, R. Ghatak, and D. R. Poddar, "Miniaturized UWB bandpass filter with dual-notch bands and wide upper stopband," *Progress In Electromagnetics Research Letters*, Vol. 38, 161–170, 2013.
2. Chu, Q.-X., X.-H. Wu, and X.-K. Tian, "Novel UWB bandpass filter using stub-loaded multiple-mode resonator," *IEEE Microw. Wireless Compon. Lett.*, Vol. 21, No. 8, 403–405, 2011.
3. Shen, Y. Z. and C. L. Law, "5.8-GHz suppressed UWB bandpass filter employing modified CRLH-TL of two and three unit cells,"

Progress In Electromagnetics Research Letters, Vol. 29, 107–113, 2012.

4. Feng, W. J., W. Q. Che, and T. Eibert, "Novel ultra-wideband bandpass filter based on transversal signal-interaction concepts," *Electron. Lett.*, Vol. 47, No. 24, 1330–1331, 2011.
5. Liu, H., T. Fu, Y. Yang, and X. Li, "Miniaturized dual-mode filter using fractal slot and snaky-shape spur-line," *Journal of Electromagnetic Waves and Applications*, Vol. 22, No. 13, 1775–1782, 2008.
6. Dai, G.-L. and M.-Y. Xia, "Novel miniaturized bandpass filters using spiral-shaped resonators and window feed structures," *Progress In Electromagnetics Research*, Vol. 100, 235–243, 2010.
7. Zhang, X. Y. and Q. Xue, "Dual-band bandpass filter using stub-loaded resonators," *IEEE Microw. Wireless. Compon. Lett.*, Vol. 17, No. 8, 583–585, 2007.
8. Gao, L. and X. Y. Zhang, "Novel dual-band bandpass filter using stub-loaded short-ended resonators," *Microw. Opt. Tech. Lett.*, Vol. 54, No. 12, 2771–2774, 2012.
9. Chen, J.-X., T. Y. Yum, J.-L. Li, and Q. Xue, "Dual-mode dual-band bandpass filter using stacked-loop structure," *IEEE Microw. Wireless Compon. Lett.*, Vol. 16, No. 9, 502–504, 2006.
10. Weng, M.-H., C.-H. Kao, and Y.-C. Chang, "A compact dual-band bandpass filter with high band selectivity using cross-coupled asymmetric SIRs for WLANs," *Journal of Electromagnetic Waves and Applications*, Vol. 24, Nos. 2–3, 161–168, 2011.
11. Hsu, C.-I. G., C.-H. Lee, and Y.-H. Hsieh, "Tri-band bandpass filter with sharp passband skirts designed using tri-section SIRs," *IEEE Microw. Wireless Compon. Lett.*, Vol. 18, No. 1, 19–21, Jan. 2008.
12. Chu, Q.-X. and X.-M. Lin, "Advanced triple-band bandpass filter using tri-section SIR," *Electron. Lett.*, Vol. 44, No. 4, 295–296, 2008.
13. Li, J. and C. L. Wei, "Compact dual-mode tri-band transversal microstrip bandpass filter," *Progress In Electromagnetics Research Letters*, Vol. 26, 161–168, 2011.
14. Chen, W. Y., M. H. Weng, S. J. Chang, H. Kuan, and Y. H. Su, "A new tri-band bandpass filter for GSM, WIMAX and ultra-wideband responses by using asymmetric stepped impedance resonators," *Progress In Electromagnetics Research*, Vol. 124, 365–381, 2012.
15. Chen, F. C. and Q. X. Chu, "Design of compact tri-band bandpass

filters using assembled resonators," *IEEE Trans. on Microw. Theory and Tech.*, Vol. 57, 165–171, 2009.

16. Luo, S., L. Zhu, and S. Sun, "Compact dual-mode triple-band bandpass filters using three pairs of degenerate modes in a ring resonator," *IEEE Trans. on Microw. Theory and Tech.*, Vol. 59, No. 5, 1222–1229, 2011.
17. Peng. Y., L. Zhang, Y. Leng, and J. Guan, "A compact tri-band passband filter based on three embedded bending stub resonators," *Progress In Electromagnetics Research Letters*, Vol. 37, 189–197, 2013.
18. Liu, Y., W.-B. Dou, and Y.-J. Zhao, "A tri-band bandpass filter realized using tri-mode T-shape branches," *Progress In Electromagnetics Research*, Vol. 105, 425–444, 2010.
19. Chen, W.-Y., M.-H. Weng, and S.-H. Chang, "A new tri-band bandpass filter based on stub-loaded step-impedance resonator," *IEEE Microw. Wireless Compon. Lett.*, Vol. 22, No. 4, 179–181, 2012.
20. Wu, H.-W. and R.-Y. Yang, "A new quad-band bandpass filter using asymmetric stepped impedance resonators," *IEEE Microw. Wireless Compon. Lett.*, Vol. 21, No. 4, 203–205, 2011.
21. Liu, J.-C., J.-W. Wang, B.-H. Zeng, and D. C. Chang, "CPW-fed dual-mode double-square-ring resonators for quad-band filters," *IEEE Microw. Wireless Compon. Lett.*, Vol. 20, No. 3, 142–144, 2010.
22. Wu. J.-Y. and W.-H. Tu, "Design of quad-band bandpass filter with multiple transmission zeros," *Electron. Lett.*, Vol. 47, No. 8, 502–503, 2011.
23. Gao, L., X. Y. Zhang, and Y.-B. Zhang, "Compact quad-band bandpass filter using open- and short-stub-loaded resonators," *Journal of Electromagnetic Waves and Applications*, Vol. 26, Nos. 8–9, 1070–1081, 2012.
24. Hong, J. S. and M. J. Lancaster, *Microwave Filters for RF/Microwave Applications*, Wiley, New York, 2011.
25. Nasrati, M. and M. Daneshmand, "Compact microstrip ultra-wideband double/single notch-band band-pass filter based on wave's cancellation theory," *IET Microwaves, Antennas & Propagation*, Vol. 6, 862–868, 2012.